IEEE Photonics Journal
An IEEE Photonics Society Publication

Super-Homogeneous Saturation of Microwave-Photonic Gain in Optoelectronic Oscillator Systems

Volume 4, Number 5, October 2012

W. Loh, Student Member, IEEE
S. Yegnanarayanan, Member, IEEE
R. J. Ram, Senior Member, IEEE
P. W. Juodawlkis, Senior Member, IEEE

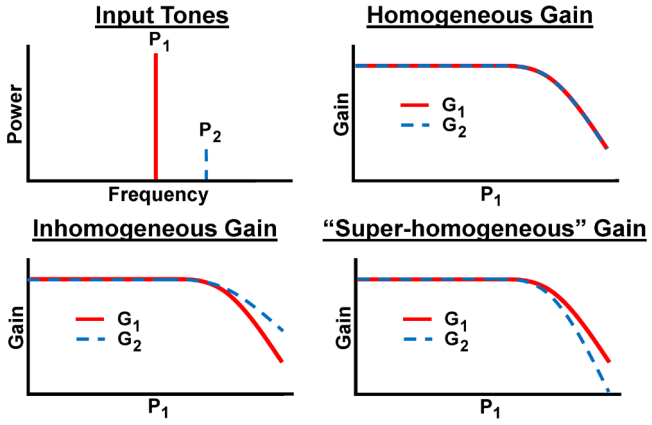

DOI: 10.1109/JPHOT.2012.2207098
1943-0655/$31.00 ©2012 IEEE

Super-Homogeneous Saturation of Microwave-Photonic Gain in Optoelectronic Oscillator Systems

W. Loh,[1,2] *Student Member, IEEE*, S. Yegnanarayanan,[1] *Member, IEEE*, R. J. Ram,[2] *Senior Member, IEEE*, and P. W. Juodawlkis,[1] *Senior Member, IEEE*

[1]Lincoln Laboratory, Massachusetts Institute of Technology, Lexington, MA 02420 USA
[2]Massachusetts Institute of Technology, Cambridge, MA 02139 USA

DOI: 10.1109/JPHOT.2012.2207098
1943-0655/$31.00 ©2012 IEEE

Manuscript received June 1, 2012; revised June 21, 2012; accepted June 27, 2012. Date of publication July 5, 2012; date of current version July 18, 2012. Corresponding author: W. Loh (e-mail: william.loh@ll.mit.edu).

Abstract: We show that the saturation characteristic of microwave-photonic gain is "super-homogeneous" such that the gain of a weaker tone saturates more rapidly than that of a stronger tone when both signals are transmitted over an intensity-modulated optical link. Using this gain model, we simulate the effect of nonlinear gain saturation on the performance of a slab-coupled optical waveguide (SCOW)-based optoelectronic oscillator (OEO). We verify our simulations with experimental measurements and show that low sidemode levels (< -110 dBc) can be achieved even when multiple modes can oscillate within the passband of the OEO loop filter.

Index Terms: Microwave photonics, Mach–Zehnder modulator, gain saturation, optoelectronic oscillators.

1. Introduction

It is well known that an intensity-modulated direct-detection (IMDD) microwave-photonic (MWP) link can achieve net electrical gain when the optical carrier power is large enough to compensate for inefficiencies in electrical-to-optical and optical-to-electrical conversion [1], [2]. Fig. 1 shows an example of an IMDD link capable of amplifying an RF input signal V_{in}. The modulator imprints the RF tone onto the envelope of an optical carrier, and the photodiode recovers the electrical signal through detection of the beat note. The amplitude of the resulting voltage V_{out} depends on the optical power incident on the photodiode, the responsivity of the photodiode, the RF load resistance (R), and also the ratio of V_{in} to the modulator half-wave switching voltage. Net electrical gain is achieved when $|V_{\text{out}}/V_{\text{in}}| > 1$. This principle of MWP gain has been used in many aspects of microwave photonics, including analog fiber-optic interconnects [1] and optoelectronic oscillators (OEOs) [3], [4]. Under small-signal conditions, often encountered in simple analog links, the MWP gain is approximately independent of the input microwave signal amplitude. However, under large-signal conditions encountered in OEOs, the gain varies as a function of input signal amplitude due to the saturation properties of the intensity modulator and the photodiode. In this paper, we assume the photodiode is linear and focus primarily on the saturation properties of the modulator. When multiple microwave signals are transmitted through a link, a phenomenon similar to cross-gain modulation can occur with each signal, not only depleting its own gain but also the gain of the others [5], [6].

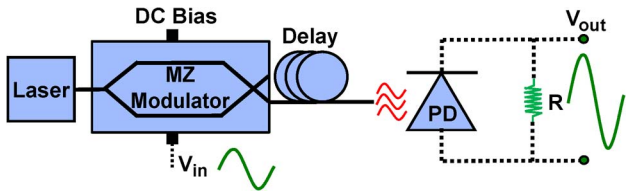

Fig. 1. MWP gain of V_{in} by signal transmission over an intensity-modulated optical link.

Previous demonstrations of OEOs have shown excellent phase-noise performance up until the offset-frequency range where sidemodes begin to dominate the spectrum [7]–[9]. Many techniques, such as the use of dual-loop [10], [11] and dual injection-locked configurations [12], have been proposed to suppress the oscillation of these sidemodes. While these approaches help to reduce spur levels, it is clear that sidemode suppression ratios (SMSRs) $>$ 50 dB can still be readily obtained even in the most basic single-loop OEO systems [8], [13]–[16]. The goal of this work is to explain how these large SMSRs can be achieved despite many (10–1000) sidemodes capable of oscillating within the passband of the OEO. In particular, we will show that the saturation behavior of MWP gain is "super-homogeneous" such that smaller signals saturate more rapidly than larger signals. The attenuation of secondary tones is particularly useful in an OEO as the sidemodes of the oscillator can be considered as unwanted noise transmitted with a primary oscillating signal. Using the model of MWP gain developed here, we simulate the steady-state operation of a high-performance slab-coupled optical waveguide optoelectronic oscillator (SCOW-OEO) system. We compare our simulation with experiment and show excellent agreement in several performance parameters, including the OEO's sidemode levels. These unique properties of MWP gain can result in large SMSRs ($>$ 110 dB), even when the filters used in the OEO support multiple cavity modes.

2. MWP Gain

To determine the behavior of the MWP gain, we first begin with the transfer function of a Mach–Zehnder (MZ) modulator derived from the Bessel expansion for two input tones [5]. The results of this expansion are well known, and the output photodetected voltage $V(t)$ can be expressed in terms of the amplitudes and frequencies of the sinusoidal inputs through

$$V(t) = \frac{P_0 \Re R}{2}\left\{1 - \cos\left[\Gamma_0 + \frac{\pi}{V_\pi}(v_1 \sin(\omega_1 t) + v_2 \sin(\omega_2 t))\right]\right\} \tag{1}$$

with

$$\cos\left[\Gamma_0 + \frac{\pi}{V_\pi}(v_1 \sin(\omega_1 t) + v_2 \sin(\omega_2 t))\right] = \sum_{n,m\geq 0}\begin{cases} \cos\Gamma_0 J_0\left(\frac{\pi v_1}{V_\pi}\right) J_0\left(\frac{\pi v_2}{V_\pi}\right) & n = m = 0 \\ (\pm 1)^n 2\cos\Gamma_0 J_n\left(\frac{\pi v_1}{V_\pi}\right) J_m\left(\frac{\pi v_2}{V_\pi}\right)\cos(n\omega_1 \pm m\omega_2)t & n+m \text{ even} \\ -(\pm 1)^{n+1} 2\sin\Gamma_0 J_n\left(\frac{\pi v_1}{V_\pi}\right) J_m\left(\frac{\pi v_2}{V_\pi}\right)\sin(n\omega_1 \pm m\omega_2)t & n+m \text{ odd.} \end{cases} \tag{2}$$

Here, P_0 is the average optical signal power at the output of the modulator, $\Re$ is the photodiode responsivity, R is the load resistance, Γ_0 is the bias point of the modulator, V_π is the modulator half-wave switching voltage, and v_1 (v_2) and ω_1 (ω_2) are the amplitudes and frequencies of the first (second) input tones, respectively.

We are specifically interested in the situation of a strong tone (v_1) and a weak tone (v_2) (see Fig. 2) corresponding to the main oscillating signal and a sidemode of an OEO. From (2), we see that one contribution to the voltage at ω_2 comes from the gain of first-order interactions obtained by substitution of $(n = 0, m = 1)$. There are also higher order interactions of ω_1 with a third tone (ω_3)

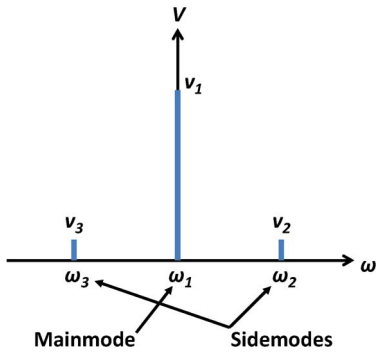

Fig. 2. Illustration of modulator input tones with mainmode (ω_1) and sidemodes (ω_2 and ω_3).

such that $2\omega_1 - \omega_3 = \omega_2$ $(n = 2, m = 1)$. In principle, (2) must be modified to account for the interaction of multiple tones. However, it can be shown that these multiple tones would simply result in additional Bessel factors in each of the expansions. For the case of the $2\omega_1 - \omega_3 = \omega_2$ interaction, the factors are $J_2(\pi v_1/V_\pi)J_0(\pi v_2/V_\pi)J_1(\pi v_3/V_\pi)$. When there is only one large signal (v_1) with multiple smaller tones as in an OEO, the factor of $J_0(\pi v_2/V_\pi)$ is approximately unity yielding again an interaction of two tones. With appropriate microwave filtering, interactions of ω_1 with frequencies near DC or with higher harmonics of the modulation signal can also be ignored. Aside from the cases of $(n = 0, m = 1)$ and $(n = 2, m = 1)$, all other interactions are negligibly small due to higher order interactions of small signals. Furthermore, for a symmetrical spectrum, the signal level at ω_3 is the same as that at ω_2. This condition approximately applies to the OEO (corresponding to the sidemodes to the left and right of the oscillating tone) and also applies to the case of signal modulation in the presence of background noise. The cross-coupling of the gain maintains amplitude symmetry between the two halves of the spectrum. Finally, we note that the voltage contribution to the signal at ω_1 comes primarily from $(n = 1, m = 0)$. All other terms are negligibly small in comparison.

In general, the contributions to $V(\omega_2)$ from the Bessel expansions with $(n = 0, m = 1)$ and $(n = 2, m = 1)$ must be incoherently summed when the signals at ω_2 and ω_3 share a random phase relation. This random phase relation is typical for describing noise and clearly applies to the case of noise transmitted alongside a modulated carrier. As will be seen later, the sidemodes of an OEO are also each phase incoherent and behave similar to noise, even when the OEO is oscillating above threshold. The lack of sidemode coherence is due to the super-homogeneous nature of MWP gain, which results in the sidemodes suffering net attenuation with each cavity roundtrip. This topic will be discussed in great detail next.

Based on our previous discussion, we can identify the signal contributions at ω_1 and ω_2 to be

$$V(\omega_1 t) = P_0 \Re R \sin\Gamma_0 J_1\left(\frac{\pi v_1}{V_\pi}\right) J_0\left(\frac{\pi v_2}{V_\pi}\right) \sin(\omega_1 t)$$

$$V(\omega_2 t) = P_0 \Re R \sin\Gamma_0 J_1\left(\frac{\pi v_2}{V_\pi}\right) \sqrt{J_0^2\left(\frac{\pi v_1}{V_\pi}\right) + J_2^2\left(\frac{\pi v_1}{V_\pi}\right)} \sin(\omega_2 t). \quad (3)$$

The form of (3) reveals saturation by cross-gain modulation as the voltages are reduced by the presence of secondary signals. Note that (3) is applicable to an approximately symmetrical spectrum with at most one dominant modulated tone. For an OEO, the assumption of a symmetrical spectrum only breaks down when the difference in spacing of ω_2 and ω_3 from ω_1 is larger than the linewidth of a sidemode. This may occur in cases of extreme mode pulling or chromatic dispersion. However, even in these situations, the spectrum analyzer performs its own incoherent addition process when the resolution bandwidth (RBW) is larger than asymmetry between ω_2 and ω_3. For asymmetries beyond these two extremes, one can proceed by modifying (3) to separately account for each voltage contribution.

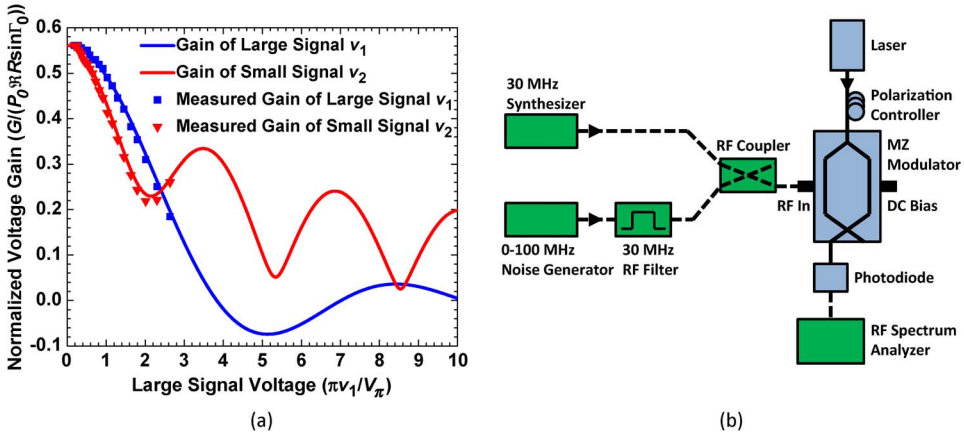

Fig. 3. (a) Simulated and experimentally measured normalized gain coefficients of two incoherent signals input on a modulator under the conditions $\pi v_2/V_\pi \ll 1$, and (b) setup for measurement of MWP gain response.

The voltage gain is found by normalization of the outputs at ω_1 and ω_2 in (3) to their respective inputs. These gains are determined to be

$$G(\omega_1 t) = \frac{P_0 \Re R}{v_1} \sin\Gamma_0 J_1\left(\frac{\pi v_1}{V_\pi}\right) \quad G(\omega_2 t) = \frac{P_0 \Re R \pi}{2V_\pi} \sin\Gamma_0 \sqrt{J_0^2\left(\frac{\pi v_1}{V_\pi}\right) + J_2^2\left(\frac{\pi v_1}{V_\pi}\right)} \tag{4}$$

where we have simplified the Bessel expansions using $J_0(\pi v_2/V_\pi) \sim 1$. Note that the voltage gain $G(\omega_2 t)$ in (4) does not contain any phase information as coherence is lost by the incoherent addition process. Should one of the terms in $G(\omega_2 t)$ dominate over the other, the phase information of the gain cannot be recovered from (4). One must use (2) to discern the phase contributed by the dominant term to $G(\omega_2 t)$.

Fig. 3(a) shows the voltage gain (normalized to $P_0 \Re R \sin\Gamma_0$) of the large and small signals as a function of the large-signal input voltage. We again wish to emphasize that phase information is lost for the gain of the small signal due to the incoherent addition of (4). We use voltage units in Fig. 3(a) primarily because they are the most natural for describing the functionality of the modulator–photodetector link. For $\pi v_1/V_\pi \ll 1$, the gains of the two tones are approximately equal as the distinction between tones 1 and 2 becomes indiscernible when they both have low amplitude. As $\pi v_1/V_\pi$ increases, Fig. 3(a) remarkably shows that the MWP gain is "super-homogeneous" with the gain of the larger signal saturating at a slower rate than the gain of the smaller signal. We note that this is distinctly different from conventional homogeneous gain where the gain saturation induced by the larger signal is the same for both signals [17]. The gain difference between the two tones continues until the primary tone reaches a value of $\pi v_1/V_\pi \approx 2.4$, at which point the secondary tone experiences larger gain. The saturation characteristics of the two tones result from the nonlinear response of the MZ modulation transfer function. The lost voltage (and power) between the two signals is accounted for by the higher order Bessel harmonics such that the sum of the contributions from all frequencies must yield the total voltage of (1) at any instant of time. In Fig. 3(a), the voltage gain coefficient of the smaller tone reaches a local minimum at $\pi v_1/V_\pi \approx 2.1$. There are also additional local minima for higher values of v_1 but with significantly reduced gain for the primary signal.

The measured MWP gain saturation for the small and large signals is also shown in Fig. 3(a). The experiment setup used for this measurement is provided in Fig. 3(b). The output of a 100 Hz–100 MHz noise generator was filtered by a bandpass filter ($f_{\text{center}} = 30$ MHz, BW $= 2$ MHz) and combined with an Agilent E8241A synthesizer. The output was applied to an MZ modulator ($V_\pi \sim 3.5$ V at 30 MHz) to drive intensity modulation of a high-power CW slab-coupled optical waveguide external cavity laser (SCOWECL) [18]. The optical signal was then detected by a

commercial Discovery photodiode (DSC20H) before subsequent analysis by an RF spectrum analyzer. The RF signal out of the synthesizer was varied between 0 and +23 dBm while the photodetected outputs at 30 and 31 MHz were monitored for the saturation measurement. The measured normalized gain compression for both the small and large signals agree well with the simulated gains for v_1 and v_2. The crossing point in gain between the two tones is clearly visible in the measurement and will become important for the discussion in the next section.

Although eqs. (1)–(4) are highly nonlinear, the super-homogeneous nature of MWP gain can be intuitively understood by a change of perspective into the frequency domain. The saturation of the larger signal occurs as a result of the modulation response generating field components at the harmonics of the modulation frequency. This is also the traditional sense of MWP saturation with the modulation signal swinging beyond the quasi-linear regime of the sinusoidal response. However, the gain saturation of the smaller signal is caused by an entirely different mechanism as the smaller signal is well within the linear range of the modulator. Ignoring the $J_2(\pi v_1/V_\pi)J_1(\pi v_3/V_\pi)$ term (which is small at relatively low v_1), the saturation of the smaller signal is due to the depletion of the field component at the carrier by the presence of the larger signal. As the field at the carrier frequency is shared by the beat note of both tones, the MWP gain of the smaller tone becomes compressed. The fact that both saturation mechanisms only depend on the larger signal makes sense in light of (4). Both the small and large tones are compressed by the shift in power from the carrier to higher harmonics of ω_1. However, because all the harmonics of ω_1 contribute to the gain of the larger tone (via beat-note generation of nearest neighbor harmonics), the gain of the larger signal saturates at a relatively slow rate. In contrast, the signal powers at harmonics of ω_1 beyond the carrier do not contribute (to first order) to the gain of the smaller signal. The only field component that contributes to gain is at the carrier frequency, which decreases rapidly to supply power to all the higher harmonics of ω_1. Compared with the larger signal then, we expect the gain of the smaller signal to initially decrease at a faster rate. Mathematically, the comparison between the saturation rates of the large and small tones becomes a comparison of $J_1(\pi v_1/V_\pi)/v_1$ to $(\pi/2V_\pi)J_0(\pi v_1/V_\pi)$ (for relatively low v_1).

3. OEO Simulation and Experimental Results

In this section, we apply (3) to the steady-state simulation of a high-performance SCOW-OEO that we have experimentally demonstrated [16]. Fig. 4 shows the schematic of the SCOW-OEO, which includes a SCOWECL and SCOW photodiode. The laser, MZ modulator, phase modulator (fiber stretcher), fiber delay, and photodiode form the IMDD link for MWP gain. The phase modulator, driven by a 60-kHz sinusoid, is used for suppression of fiber nonlinearities (stimulated Brillouin scattering and double backscattered interferometric noise) during signal propagation through the delay [7], [22]. The signal at the input of the modulator is amplified by the IMDD link and filtered during one roundtrip of the cavity. If the gain is large enough to compensate for the loop losses, the OEO will oscillate at the center frequency determined by the RF filter.

The simulation is performed by iterating over successive roundtrips of the OEO, each time updating the signal voltage. Starting from noise (thermal noise, shot noise, and laser RIN), we use (3) to calculate the voltage amplified by one roundtrip of the MWP link. Next, we incoherently add noise to the resulting voltage and iterate the process over 1000 roundtrips of the cavity. In each iteration, we monitor the intracavity power and gain of both the mainmode and sidemode. Mathematically, the power in the mainmode or sidemode after the Nth roundtrip $(P_{\mathrm{RF},N})$ can be expressed as $P_{\mathrm{RF},N} = P_{\mathrm{RF},N-1}G + P_{\mathrm{Noise}}$. Here, $P_{\mathrm{RF},N-1}$ is the power of the previous roundtrip, G is the equivalent MWP power gain [obtained using (3)] for the mainmode or sidemode, and P_{Noise} is the added contribution due to thermal noise, shot noise, and laser RIN. The measured losses of the RF loop were included as direct losses to the voltage gain and injected noise. Table 1 summarizes the experimentally measured parameters used in the OEO simulation. It should be emphasized that no fitting parameters were used for the simulation of the SCOW-OEO. In the first iteration only, we introduce a $\sim$1 dB noise spike between the noise at frequencies ω_1 and ω_2. As will be shown later,

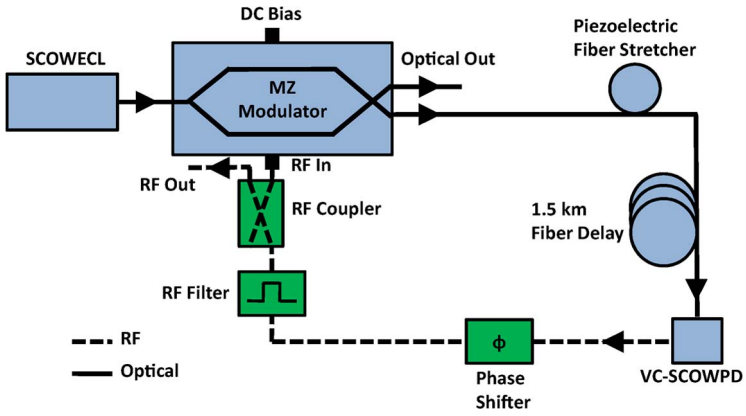

Fig. 4. Schematic of SCOW-OEO configuration used in simulation and experimental measurement.

TABLE 1

Experimentally measured MWP link parameters used for simulation of the SCOW-OEO

Parameter	Value
RF Loss (α_{RF})	4.9 dB
Responsivity ($\Re$)	1 A/W
Modulator V_{Π}	3.1 V
Characteristic Impedance (R)	50 Ω
Modulator Bias Point (Γ_0)	58°
Relative Intensity Noise (RIN)	-160 dBc/Hz
Optical Loss After Modulator (α_{Op})	1.5 dB

this difference in injected noise is enough to cause the system to evolve to a state where the larger signal dominates.

In general, noise processes are referenced to a 1-Hz bandwidth and must be scaled appropriately to the bandwidth of the oscillating signal of interest. However, for the purposes of simulation, it does not matter what scaling factor is chosen as the convergence of the simulation only depends on the parameters of Table 1. The steady-state behavior is independent of input conditions as long as both input tones are initially small, and one tone starts larger than the other (by means of noise fluctuation). The input tones continue to receive gain (or loss) from the system until the modulation Bessel-function response saturates. For ease of simulation, we use a 1-Hz noise bandwidth. After 1000 iterations, the simulation quickly converges to steady state.

From the simulation, many aspects regarding the OEO's steady-state operation can be predicted. Fig. 5(a) shows the RF power of the two tones at steady state graphed as a function of the DC photocurrent [determined using (2) with $n = m = 0$]. Starting with just a small difference in noise during the first iteration, the system evolves such that the stronger (mainmode) tone receives all of the signal power above threshold. Below threshold, the mainmode and sidemode (weaker tone) RF powers are similar. The simulation reaches oscillation threshold at 19 mA, which matches our experimentally observed threshold photocurrent of $\sim$20 mA. Beyond threshold, the simulated RF power is 9.3 mW at 27.3-mA photocurrent operation. Experimentally, we measure 1-mW output from a $-$10-dB coupler when the SCOW-OEO was operated at 27.3 mA. This corresponds to $\sim$9-mW intracavity power after accounting for output losses and thus agrees well with our simulated RF power.

Fig. 5(b) shows the evolution of the mainmode and sidemode power gain as a function of the DC photocurrent. Here, we graph the gain of RF power (instead of voltage) as an aid for the discussion of sidemode suppression next. Below threshold, the gain of the mainmode and sidemode is similar

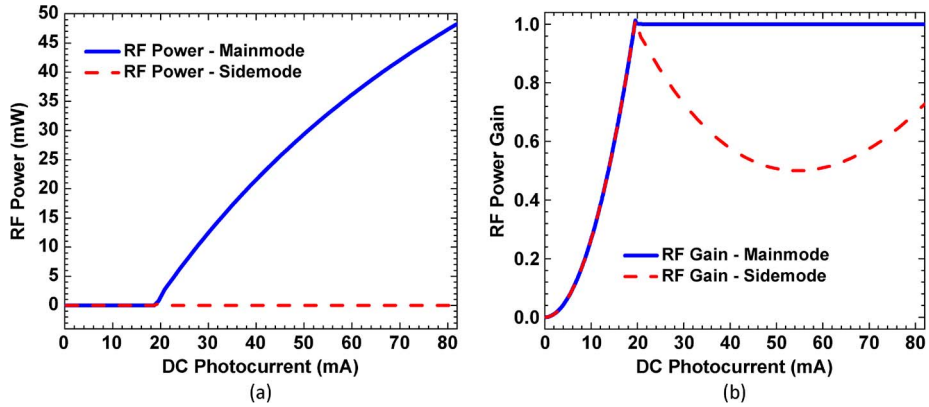

Fig. 5. Simulated SCOW-OEO (a) RF power and (b) RF power gain as a function of DC photocurrent for mainmode and sidemode tones.

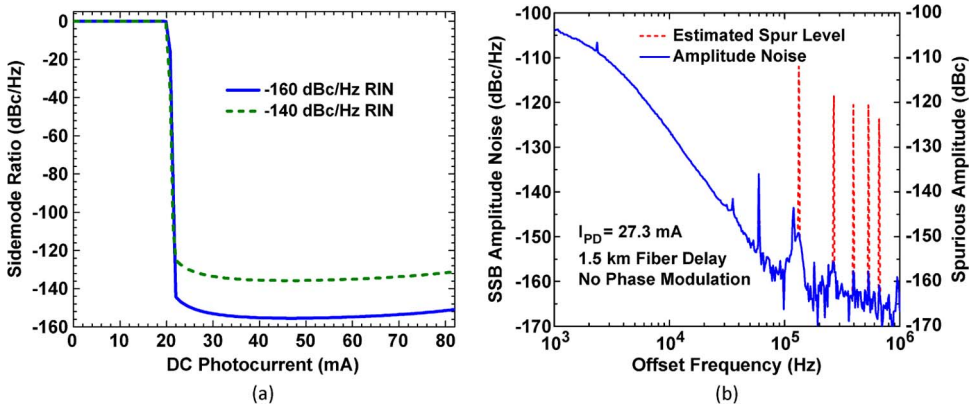

Fig. 6. (a) Simulated SCOW-OEO SMSR in dBc/Hz as a function of DC photocurrent for laser RIN of −160 dBc/Hz (solid line) and −140 dBc/Hz (dashed line) and (b) measured SCOW-OEO amplitude-noise spectrum with estimated sidemode spur levels indicated.

as both tones are small signal and nearly indistinguishable in (3). Once the mainmode reaches a gain of 1, the system oscillates and builds up power into the mainmode. As power continues to increase with photocurrent, the sidemode gain decreases according to the behavior determined in Fig. 3(a) for a single roundtrip. Fig. 5(b) shows that a large gain differential can be achieved resulting solely from the nonlinear transfer function of the modulator. At 27.3-mA operation, we simulate the gain differential of the SCOW-OEO to be 0.79. The sidemode gain begins to increase again past 54 mA due to the inherent nonlinearity of the modulator Bessel transfer function. Beyond 80 mA, eventually, the sidemode gain becomes larger than the mainmode gain causing multimode operation of the OEO.

The SMSR can now be calculated as the ratio of the sidemode power to the mainmode power. Here, the choice of noise bandwidth influences the result as the steady-state power of the sidemode tone depends on its initial conditions. The reason for this is because the sidemode tone operates below threshold and attenuates after each roundtrip. The steady-state sidemode RF power is thus the power accumulated from its last few roundtrips within the OEO cavity. This power is expected to be proportional to the level of the injected noise during each iteration, and therefore, the SMSR varies with these input conditions. Instead of calculating the total ratio of sidemode and mainmode powers, we first simulate the sidemode ratio per hertz bandwidth [see Fig. 6(a)]. We later calculate the total mode power by integrating the sidemode suppression over the linewidth of the mode.

Fig. 6(a) indicates that the sidemode ratio is 0 dBc/Hz below threshold. This is expected as the mainmode and sidemode levels are similar before the OEO can oscillate. At 27.3 mA, the sidemode ratio is simulated to be −152 dBc/Hz (solid line). The RIN used for this simulation was −160 dBc/Hz, which is the measured SCOWECL RIN for offset frequencies (100 kHz–1 MHz) [16]. Injection of shot noise and thermal noise was also accounted for in the simulation. The linewidth (Δf) of a sidemode can be calculated from the cavity quality factor through [19]

$$\Delta f = \frac{\delta_c}{2\pi T_{rt}} \quad \delta_c = \ln\left(\frac{1}{g_{rt}}\right) \tag{5}$$

where T_{rt} is the roundtrip time, and g_{rt} is the power gain of a sidemode per roundtrip. Since g_{rt} is limited to be <1, the linewidth of the cavity modes will be finite. Using $g_{rt} = 0.79$, we find $\Delta f \sim 5.1$ kHz. Multiplying the sidemode ratio by the 5.1-kHz linewidth, we calculate the total sidemode power relative to the mainmode to be −115 dBc. Fig. 6(b) shows the amplitude-noise spectrum of the SCOW-OEO system measured using an Agilent E5052B signal-source analyzer (SSA). Phase modulation is commonly applied to OEOs to suppress nonlinear noise processes due to signal propagation over optical fiber. Phase modulation was not applied here to prevent confusion between spurious tones and sidemodes. In the offset-frequency range 100–780 kHz, the RBW setting is 3.1 kHz. Since the RBW is similar to the linewidth of a sidemode, the calculated sidemode ratio can be directly compared with the measured spur levels (in dBc/Hz) without suffering too much accuracy loss integrating over noise. For the purposes of this comparison, we assume the power in the sidemode is evenly divided between amplitude and phase. We thus subtract 3 dB from our simulated sidemode ratio for comparison to the measured sidemodes in the amplitude-noise spectrum. This value (−155 dBc/Hz) agrees well with the baseline sidemode levels (solid line) measured at harmonics of ∼135 kHz. In Fig. 6(b), spurious detection was used to detect the ratio of total sidemode power relative to the mainmode. We calibrated this measurement against spurs from an external source as the SSA could not directly detect the sidemode peaks. The dashed lines in Fig. 6(b) indicate the estimated level of the OEO amplitude-noise sidemodes and agree with the simulated amplitude-noise sidemodes (−118 dBc) after accounting for the 3-dB phase-noise contribution. In principle, the sidemode levels can also be determined from a measurement of the SCOW-OEO's phase-noise spectrum. However, these sidemodes are at the level of the noise floor for the SSA's phase-noise measurement.

Note that our simulation of sidemode ratio in Fig. 6(a) did not assume any RF filter bandwidth to reject the sidemodes. The low sidemode levels achieved are solely due to the gain differential introduced by the nonlinear modulation properties of MWP gain. With further increase in photocurrent, we find that the sidemode ratio decreases toward the level of the injected noise (normalized to the noise bandwidth). That is, as the gain difference between mainmode and sidemode increases further, the contribution to the sidemode power approaches the limit set by the injected noise for a single roundtrip. Fig. 6(a) also shows the simulated sidemode ratio with a RIN noise injection level of −140 dBc/Hz. This represents the RIN performance of conventional semiconductor, fiber, and solid-state lasers at ∼100-kHz offset frequency [7]. In Fig. 6(a), the sidemode ratio degrades by 20 dB, corresponding to the 20-dB increase in noise injection. The increase in sidemode levels in direct proportion to the noise injection level is expected in light of our previous discussion on the impact of noise bandwidth. To provide further intuition, we note that the simulation process (below threshold) of multiplying by the gain and adding noise with each iteration step resembles the propagation of amplified spontaneous emission (ASE) through an optical amplifier. The total ASE at the output of the amplifier can be integrated, and the resulting expression is also directly proportional to the amplifier's spontaneous emission noise injection [20]. Finally, the dependence of the sidemodes on RIN can also be seen in [7, Fig. 6]. The low RIN of the SCOW lasers is the primary reason why the SCOW-OEO exhibits much lower sidemode levels compared with typical OEOs. However, we find the removal of the RF amplifier to also be beneficial for sidemode reduction [16], [21].

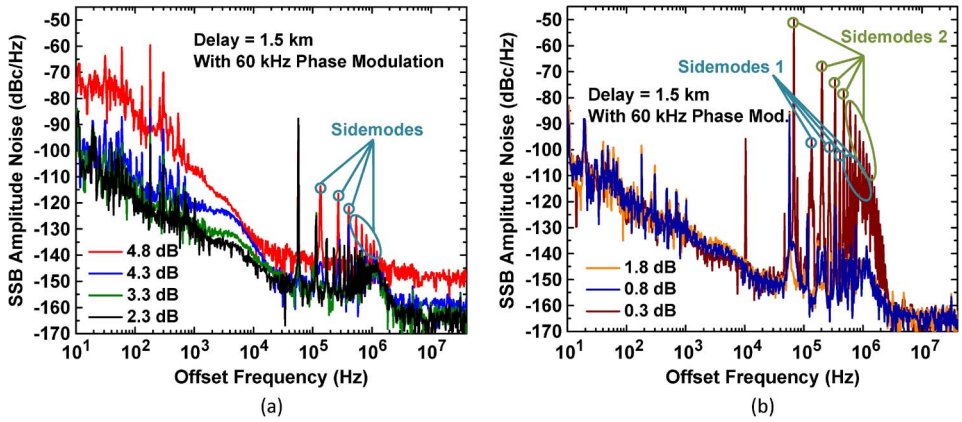

Fig. 7. Measured SCOW-OEO single-sideband (SSB) amplitude-noise spectrum under (a) 4.8–2.3-dB and (b) 1.8–0.3-dB optical power attenuation.

It is tempting to apply (3) to the case when the OEO is operated in deep saturation (DC photocurrent > 90 mA). At these limits, the sidemode gain becomes larger than the mainmode gain, and the assumption of one large signal oscillating in the presence of multiple smaller signals breaks down. One can potentially obtain corrections to the gain response by expanding (3) to include third-order Bessel interactions between the modes of the OEO (second-order interactions are small due to the RF filter). Doing so, we find that the sidemodes increase rapidly toward the level of the mainmode in the deep-saturation limit. Higher order Bessel interactions are required in order to simulate the behavior of the OEO beyond these extremes.

The behavior of the OEO in the high saturation limit can be experimentally determined by increasing the gain through use of RF amplification in the cavity (see Fig. 7). For our SCOW-OEO system, we use an AML26PNA1811 low phase-noise amplifier with $G \sim 23$ dB and $P_{\text{sat}} \sim 25$ dBm. We also use a variable optical attenuator after the laser in order to control the total MWP gain within the OEO cavity. The optical attenuation is varied between 4.8 and 0.3 dB for the measurement in Fig. 7. At 4.8-dB attenuation, the OEO operates just above threshold and exhibits significantly larger amplitude noise compared with the rest of the cases. However, over much of the frequency range (> 30 kHz), we expect the baseline noise floor to be measurement limited. The SSA measurement noise floor depends on the input RF signal level and is near its sensitivity limit when the OEO oscillates just above threshold. This can be seen above 2 MHz where no rollover in the amplitude noise is observed, even past the RF filter cutoff. The first sidemode spur is located at 135-kHz offset at a level of ~ -114 dB/Hz and is clearly above the system noise floor. The other sidemodes can also be observed but are difficult to isolate from the 60-kHz phase modulation spurs.

As the attenuation is lowered, the sidemode levels can be observed to decrease (relative to the mainmode) at all frequencies within the spectrum. This improvement in SMSR is due to "super-homogeneous" saturation of MWP gain in the SCOW-OEO. At ~2.3-dB attenuation, the sidemodes decrease to the level of noise (−155 dBc/Hz) and are masked in the amplitude-noise spectrum. This continues until the attenuation reaches 0.8 dB, at which point the sidemodes begin to grow. Interestingly, the sidemodes are located at offset frequencies of 67.5 kHz, 202.5 kHz, 337.5 kHz, etc. and appear to be shifted by half the free spectral range (FSR) relative to the mainmode. Upon reaching 0.3-dB attenuation, the sidemodes experience exponential growth and increase toward the level of the oscillating signal. At this attenuation level, the condition $\pi v_1 / V_\pi \approx 2.4$ is satisfied, and the sidemode gain becomes equal to the mainmode gain. From the total detected RF power (~9.0 dBm) output from the 10-dB coupler, we find $\pi v_1 / V_\pi \sim 2.67$, which agrees with theory. It appears that two distinct sets of sidemodes form, starting at 67.5- and 135-kHz offset frequency and periodic at intervals of the FSR (135 kHz). However, the modes located at harmonics of 135 kHz are created by difference frequency generation due to the 67.5-kHz sidemodes after modulation. This can be verified through evaluation of how the modes scale with optical attenuation or by simple

observation of the power level difference between each set of modes. Any multiple of 135 kHz can be generated between any two sidemodes as the modes are spaced by the FSR of the cavity. Similarly, the signal at ~10 kHz is created by the difference frequency between the first sidemode (67.5 kHz) and the phase modulation tone (57.5 kHz).

It is interesting to discuss the origin of the phase shift, which results in sidemodes located half an FSR closer to the oscillating signal. As one FSR corresponds to 2π phase shift, the total phase shift experienced by each sidemode is π. This π phase shift can be interpreted from the gain curve in Fig. 3(a). The gain was determined by an incoherent addition of voltage between sidemodes located at identical frequency offsets from the oscillating mode. The phase information of the voltage signal is lost after this incoherent addition, and the voltage gain becomes just an expression related to the power gain. However, at the point where $\pi v_1/V_\pi \approx 2.4$ is reached, $J_0(\pi v_1/V_\pi)$ is over two orders of magnitude lower than $J_2(\pi v_1/V_\pi)$ and, thus, can be ignored in the expression for gain in (4). The remaining contribution of $J_2(\pi v_1/V_\pi)J_1(\pi v_2/V_\pi)$ to sidemode gain is always opposite in sign to the voltage gain of the primary mode $(J_1(\pi v_1/V_\pi)J_0(\pi v_2/V_\pi))$, as can be seen in (2). This introduces an extra π phase shift in the gain of the sidemodes relative to the gain of the mainmode. Since the roundtrip phase shift of a sidemode must be a multiple of 2π to maintain self-coherence, the significance of the π phase shift is to shift the sidemodes half an FSR closer to the oscillating mode.

4. Conclusion

We have shown that the MWP gain is "super-homogeneous" such that the stronger signal saturates the gain of the weaker signal more than the saturation of its own gain. This concept has been applied to the simulation of an OEO for determination of its steady-state operation. Without any fitting parameters, the simulation agrees well with experimental measurements of the SCOW-OEO's steady-state operation. We show theoretically and experimentally that excellent SMSRs of $>$ 110 dBc can be achieved despite the presence of multiple modes within the OEO cavity. However, the same nonlinear MWP gain properties that result in large OEO sidemode suppressions also cause multimode operation when the oscillation signal becomes too large. At these limits, the sidemodes undergo a frequency shift of half the FSR relative to the mainmode oscillation. These unique properties of the MWP gain may find other practical applications in the design of opto-electronic systems.

References

[1] C. H. Cox, *Analog Optical Links Theory and Practice*. Cambridge, U.K.: Cambridge Univ. Press, 2004.
[2] W. S. Chang, *RF Photonic Technology in Optical Fiber Links*. Cambridge, U.K.: Cambridge Univ. Press, 2002.
[3] X. S. Yao and L. Maleki, "Optoelectronic microwave oscillator," *J. Opt. Soc. Amer. B*, vol. 13, no. 8, pp. 1725–1735, Aug. 1996.
[4] X. S. Yao and L. Maleki, "Optoelectronic oscillator for photonic systems," *IEEE J. Quantum Electron.*, vol. 32, no. 7, pp. 1141–1149, Jul. 1996.
[5] B. H. Kolner and D. W. Dolfi, "Intermodulation distortion and compression in an integrated electrooptic modulator," *Appl. Opt.*, vol. 26, no. 17, pp. 3676–3680, Sep. 1987.
[6] R. Olshansky, "Optimal design of subcarrier multiplexed lightwave systems employing linearized external modulators," *IEEE J. Lightw. Technol.*, vol. 10, no. 3, pp. 378–382, Mar. 1992.
[7] D. Eliyahu, D. Seidel, and L. Maleki, "RF amplitude and phase-noise reduction of an optical link and an opto-electronic oscillator," *IEEE Trans. Microw. Theory Tech.*, vol. 56, no. 2, pp. 449–456, Feb. 2008.
[8] D. Eliyahu, D. Seidel, and L. Maleki, "Phase noise of a high performance OEO and an ultra low noise floor cross-correlation microwave photonic homodyne system," in *Proc. IEEE FCS*, 2008, pp. 811–814.
[9] C. W. Nelson, A. Hati, and D. A. Howe, "Relative intensity noise suppression for RF photonic links," *IEEE Photon. Technol. Lett.*, vol. 20, no. 18, pp. 1542–1544, Sep. 2008.
[10] X. S. Yao and L. Maleki, "Ultralow phase noise dual-loop optoelectronic oscillator," in *Proc. OFC*, 1998, pp. 353–354.
[11] W. Zhou, O. Okusaga, C. Nelson, D. Howe, and G. Carter, "10 GHz dual loop opto-electronic oscillator without RF-amplifiers," in *Proc. SPIE*, 2008, pp. 68970Z-1–68970Z-6.
[12] W. Zhou and G. Blasche, "Injection-locked dual opto-electronic oscillator with ultra-low phase noise and ultra-low spurious level," *IEEE Trans. Microw. Theory Tech.*, vol. 53, no. 3, pp. 929–933, Mar. 2005.
[13] C. W. Nelson, A. Hati, D. A. Howe, and W. Zhou, "Microwave optoelectronic oscillator with optical gain," in *Proc. FCS*, 2007, pp. 1014–1019.

[14] W. Li and J. Yao, "An optically tunable optoelectronic oscillator," *IEEE J. Lightw. Technol.*, vol. 28, no. 18, pp. 2640–2645, Sep. 2010.
[15] A. Hayat, A. Bacou, A. Rissons, and J.-C. Mollier, "2.49 GHz low phase-noise optoelectronic oscillator using 1.55 μm VCSEL for avionics and aerospace applications," in *Proc. SPIE*, 2009, p. 722 90O-8.
[16] W. Loh, J. Klamkin, S. M. Madison, F. J. O'Donnell, J. J. Plant, S. Yegnanarayanan, R. J. Ram, and P. W. Juodawlkis, "Slab-coupled optical waveguide (SCOW) based optoelectronic oscillator (OEO)," in *Proc. IEEE IPC*, 2011, pp. 605–606.
[17] T. D. Anh and W. Dietel, "Homogeneous broadening in a 0.63 μm single mode He–Ne laser," *Opt. Quantum Electron.*, vol. 5, no. 3, pp. 243–248, May 1973.
[18] W. Loh, F. J. O'Donnell, J. J. Plant, M. A. Brattain, L. J. Missaggia, and P. W. Juodawlkis, "Packaged, high-power, narrow-linewidth slab-coupled optical waveguide external cavity laser (SCOWECL)," *IEEE Photon. Technol. Lett.*, vol. 23, no. 14, pp. 974–976, Jul. 2011.
[19] A. E. Siegman, *Lasers*. Mill Valley, CA: Univ. Sci. Books, 1986.
[20] W. Loh, J. J. Plant, J. Klamkin, J. P. Donnelly, F. J. O'Donnell, R. J. Ram, and P. W. Juodawlkis, "Noise figure of watt-class ultralow-confinement semiconductor optical amplifiers," *IEEE J. Quantum Electron.*, vol. 47, no. 1, pp. 66–75, Jan. 2011.
[21] W. Loh, S. Yegnanarayanan, J. Klamkin, S. M. Madison, J. J. Plant, F. J. O'Donnell, and P. W. Juodawlkis, "Amplifier-free slab-coupled optical waveguide optoelectronic oscillator systems," to be published.
[22] P. K. Pepeljugoski and K. Y. Lau, "Interferometric noise reduction in fiber-optic links by superposition of high frequency modulation," *IEEE J. Lightw. Technol.*, vol. 10, no. 7, pp. 957–963, Jul. 1992.